J Mol Model (2011) 17:1831–1840
DOI 10.1007/s00894-010-0873-7

ORIGINAL PAPER

Identification of novel 5-hydroxy-1*H*-indole-3-carboxylates with anti-HBV activities based on 3D QSAR studies

Hui-fang Chai · Xin-xia Liang · Lin Li · Chun-shen Zhao · Ping Gong · Zhong-jie Liang · Wei-liang Zhu · Hua-liang Jiang · Cheng Luo

Received: 19 April 2010 / Accepted: 8 October 2010 / Published online: 30 October 2010
© Springer-Verlag 2010

Abstract Infection with hepatitis B virus (HBV) is a major cause of liver diseases such as cirrhosis and hepatocellular carcinoma. In our previous studies, we identified indole derivatives that have anti-HBV activities. In this study, we optimize a series of 5-hydroxy-1*H*-indole-3-carboxylates, which exhibited potent anti-HBV activities, using three-dimensional quantitative structure-activity relationship (3D QSAR) studies with comparative molecular field analysis (CoMFA) and comparative molecular similarity indices analysis (CoMSIA). The lowest energy conformation of compound **3**, which exhibited the most potent anti-HBV activity, obtained from systematic search was used as the template for alignment. The best predictions were obtained with the CoMFA standard model (q^2=0.689, r^2 = 0.965, SEE=0.082, F=148.751) and with CoMSIA combined steric, electrostatic, hydrophobic and H-bond acceptor fields (q^2=0.578, r^2=0.973, SEE=0.078, F=100.342). Both models were validated by an external test set of six compounds giving satisfactory prediction. Based on the clues derived from CoMFA and CoMSIA models and their contour maps, another three compounds were designed and synthesized. Pharmacological assay demonstrated that the newly synthesized compounds possessed more potent anti-HBV activities than before (IC_{50}: compound **35a** is 3.1 μmol/l, compound **3** is 4.1 μmol/l). Combining the clues derived from the 3D QSAR studies and from further validation of the 3D QSAR models, the activities of the newly synthesized indole derivatives were well accounted for. Furthermore, this showed that the CoMFA and CoMSIA models proved to have good predictive ability.

Keywords Anti-HBV · Anti- hepatitis B virus activity · CoMFA · CoMSIA · Indole derivatives · QSAR · Synthesis · 3D QSAR

Hui-fang Chai, Xin-xia Liang, Lin Li and Chun-shen Zhao contributed equally to this work.

H.-f. Chai (✉)
Department of Pharmacy,
Guiyang College of Traditional Chinese Medicine,
Guiyang 550002, China
e-mail: saieho@126.com

X.-x. Liang · C.-s. Zhao
Guizhou Province Key Laboratory of Fermentation Engineering and Biological Pharmacy, Guizhou University,
Guiyang 550003, China

L. Li
Division of Nephrology, Shanghai Changzheng Hospital,
Shanghai 200003, China

P. Gong
School of Pharmaceutical Engineering,
Shenyang Pharmaceutical University,
Shenyang 110016, China

Z.-j. Liang · W.-l. Zhu · H.-l. Jiang · C. Luo
Drug Discovery and Design Center,
State Key Laboratory of Drug Research, Shanghai Institute of Materia Medica, Chinese Academy of Sciences,
Shanghai 201203, China

H.-l. Jiang
e-mail: hljiang@mail.shcnc.ac.cn

C. Luo
e-mail: cluo@mail.shcnc.ac.cn

Introduction

Hepatitis B virus (HBV) infection is a major cause of liver diseases such as cirrhosis and hepatocellular carcinoma. Recent reports show that more than 400 million people are chronically infected with HBV worldwide and about 1

million people are estimated to die of HBV-infected diseases every year [1, 2]. Clinical therapies for HBV infections include interferon, nucleoside analogues lamivudine and adefovir dipivoxil. However, because of low clinical response rates (in the cases of interferon-α and peginterferon-α) or inevitable drug-resistance, the current regimens are far from satisfactory [3–5]. New anti-HBV drugs with novel mechanisms of action are urgently needed.

Previously, our group has carried out studies to find more potent anti-HBV derivatives and obtained several new compounds possessing anti-HBV activities [6–8]. In that report, we described a series of 6-bromo-5-hydroxy-1*H*-indole-3-carboxylate with favorable anti-HBV activities ex vivo [6]. Furthermore, some novel ethyl 5-hydroxy-1*H*-indole-3-carboxylate derivatives were synthesized in which the bromine in position 6 of the indole ring was substituted by hydrogen [7, 8]. Unfortunately, not enough work was done at the time to be able to summarize the structure-activity relationship (SAR) of the indole derivatives. Hence, it is necessary to construct QSAR models to get further insights into the relationship between the molecular structures and bioactivities for designing new anti-HBV compounds. In this paper, we report our 3D QSAR models, including CoMFA and CoMSIA studies, based on 26 compounds reported earlier. Based on the clues derived from QSAR models, three new compounds were designed and synthesized. The pharmacological assay showed that the newly synthesized derivatives possessed anticipated anti-HBV activities. Our models proved to have good predictive ability and to be consistent with the experimental data, thereby lighting up the road to design new analogues with anti-HBV activity.

Materials and methods

Three dimensional quantitative structure-activity relationship (3D QSAR)

3D QSAR analysis for anti-HBV activities of the indole derivatives was performed in order to correlate the biochemical data with chemical formulas, and to identify positive and negative structural features within the reported compounds.

Computational details

Data set

26 compounds were employed in this study, which were from references 6-8 and several unreported molecules synthesized previously by our colleagues. Their structures and bioactivities were listed in Table 1. For 3D QSAR analyses, 20 compounds (compound **1**-**20** in Table 1) were selected as a training set for model construction. The prediction of the derived model was evaluated using an external test set of six compounds (compound **21**-**26** in Table 1) randomly selected. The anti-HBV data input was represented by pIC_{50} (Log $(1/IC_{50})$, IC_{50} is mol/l).

Molecular structures

All molecular modeling calculations were performed using SYBYL 6.8 software package on SGI Origin 3800 workstation [9]. The 3D molecular structures were constructed by using sketch module. Energy minimizations were performed on compounds **1**-**26** using the Tripos force field and Gasteiger-Hückel charge with distance dependent dielectric and conjugate gradient method with convergence criterion of 0.01 $kcal\,mol^{-1}$.

Molecular alignment

It is the most important requirement for CoMFA and CoMSIA studies that the 3D structures to be analyzed are aligned according to a suitable conformational template, which is typically assumed to be a 'bioactive' conformation. Since no structural information on ligand-receptor complexes is available, the lowest energy conformation of compound **3** obtained from the random search option given in SYBYL, which also exhibited the most potent anti-HBV activity, was used as template structure for the alignment. All the molecules of the training set were aligned on the template molecule by using the simple 'align database' option given in SYBYL. Alignment and atoms used for superimposition were shown in Fig. 1.

CoMFA

Steric and electrostatic interactions were calculated using a sp^3 carbon atom as a steric probe and a +1 charge as an electrostatic probe with Tripos force field. The CoMFA grid spacing used was 2.0 Å in the *x*, *y* and *z* directions, and the grid region was automatically generated by the CoMFA routine to encompass all molecules with an extension of 4.0 Å in each direction. The default value of 30 $kcal\,mol^{-1}$ was set as the maximum steric and electrostatic energy cutoff. Minimum-sigma (column filtering) was set to be 2.0 $kcal\,mol^{-1}$ to improve the signal-to-noise ratio by omitting those lattice points, whose energy variation is below this threshold. Regression analysis was performed using the partial least square (PLS) algorithm. The final model was developed with the optimum number of components equal to that yielding the highest q^2.

Table 1 Structures and anti-HBV activities of ethyl 5-hydroxy-1*H*-indole-3-carboxylates derivatives

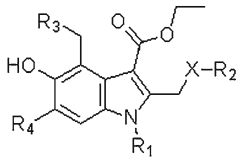

5-hydroxy-1H-indole-3-carboxylates

Compound.	R_1	R_2	R_3	R_4	X	IC_{50} (μM)
1	Methyl	*m*-Methylphenyl	Dimethylamino	Bromo	Sulfinyl	61.1
2	Methyl	*m*-Methoxyphenyl	Dimethylamino	Bromo	Sulfinyl	39.3
3	Methyl	*m*-Methoxyphenyl	Dimethylamino	Bromo	Sulfonyl	4.1
4	Methyl	*m*-Methoxyphenyl	Pyrrolidinyl	Hydrogen	Sulfonyl	31.7
5	Methyl	*o*-Methylphenyl	Morpholino	Bromo	Sulfinyl	30.9
6	Methyl	*p*-Fluorophenyl	Morpholino	Bromo	Sulfinyl	104.3
7	Methyl	*m*-Chlorophenyl	Morpholino	Bromo	Sulfinyl	46.6
8	Methyl	*p*-Methylphenyl	4'-Methylpiperazinyl	Hydrogen	Sulfinyl	48.2
9	Methyl	*m*-Methoxyphenyl	4'-Methylpiperazinyl	Hydrogen	Sulfinyl	49.2
10	Cyclopropyl	*m*,*p*-Difluorophenyl	4'-Methylpiperazinyl	Bromo	Sulfinyl	8.9
11	Methyl	*p*-Methylphenyl	Guanidinyl	Bromo	Sulfinyl	19.6
12	Methyl	*p*-Fluorophenyl	Guanidinyl	Bromo	Sulfinyl	56.0
13	Cyclopropyl	*p*-Fluorophenyl	Guanidinyl	Bromo	Sulfinyl	9.4
14	Methyl	Phenyl	Imidazolyl	Bromo	Sulfinyl	5.0
15	Methyl	*o*-Fluorophenyl	Imidazolyl	Bromo	Sulfinyl	16.5
16	Methyl	*p*-Fluorophenyl	Imidazolyl	Bromo	Sulfinyl	25.4
17	Cyclopropyl	*p*-Fluorophenyl	Imidazolyl	Bromo	Sulfinyl	20.3
18	Methyl	Phenyl	2'-Methylimidazolyl	Bromo	Sulfinyl	42.5
19	Methyl	*o*-Methoxyphenyl	2'-Methylimidazolyl	Bromo	Sulfinyl	4.3
20	Methyl	Phenyl	Triazolyl	Bromo	Sulfinyl	25.3
21	Methyl	*m*-Fluorobenzyl	Dimethylamino	Bromo	Sulfinyl	11.6
22	Methyl	*p*-Fluorobenzyl	Pyrrolidinyl	Bromo	Sulfonyl	10.2
23	Methyl	Phenyl	2'-Methylimidazolyl	Bromo	Sulfonyl	13.7
24	Methyl	*m*,*p*-Difluorophenyl	2'-Methylimidazolyl	Bromo	Sulfinyl	11.3
25	Methyl	*m*-Chloro, *p*-Fluorophenyl	2'-Methylimidazolyl	Bromo	Sulfinyl	76.0
26	Cyclopropyl	*o*-Methylphenyl	Dimethylamino	Bromo	Sulfinyl	48.6

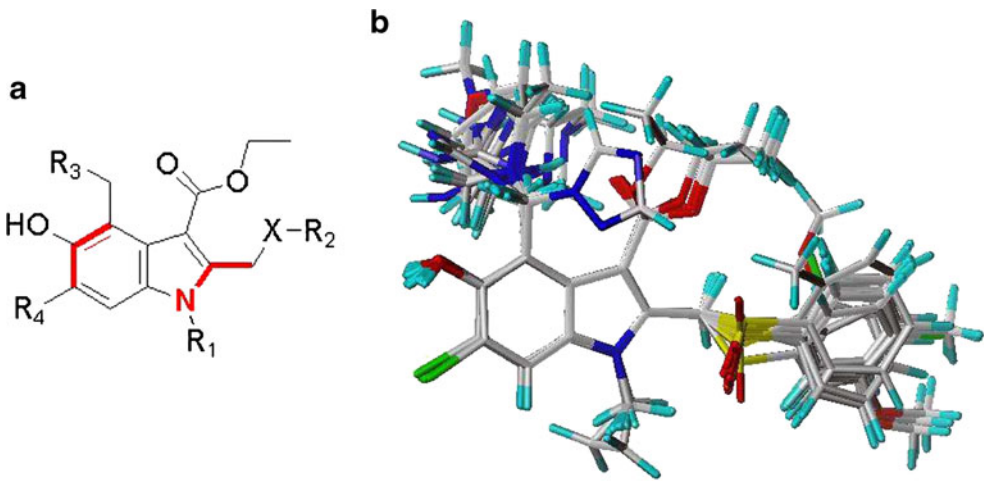

Fig. 1 (**a**) Template used for alignment (reference atoms are shown in red bold). (**b**) Training set aligned on minimum energy conformation of compound **3**

CoMSIA

The alignment model used in CoMFA study was adopted for CoMSIA as well. Four physicochemical properties: the steric, electrostatic, hydrophobic and H-bond acceptor fields, were evaluated. The steric contribution was proportional to the third power of the atomic radii of the atoms. Electrostatic properties have been introduced as Gasteiger-Masili charges. An atom based hydrophobicity was estimated according to the parameterization developed by Ghose and co-workers [10]. The lattice dimensions were selected with a sufficiently large margin (4 Å) to enclose all aligned molecules as in CoMFA. Similarity indices were computed using a probe with a charge of +1, a radius of +1 Å, a hydrophobicity of +1, and 0.3 as the attenuation factor α for the Gaussian-type distance. The statistical evaluation for the CoMSIA analyses were performed in the same way as described for CoMFA.

Synthesis and biological assay

Synthetic details

Synthetic route

The synthesis of target compounds was achieved using a convenient route started from the commercially available compound **27** and alkylamine, followed by the Nenitsescu condensation of compound **28** and 1,4-benzoquinone [11]. Acetyl chloride was then added into the solution of compound **29** and pyridine to protect the hydroxy group in position 5 of the indole ring, to give compound **30** with a yield of 87%. Compound **30** was transformed into compound **32** by two steps of bromination and a reaction with the appropriate arylthiol. According to the procedure of Grinev and Pershin, we obtained compounds **33a-c** by the Mannich reaction of compound **32** with dimethylamine [12]. 2-Methylimidazole or guanidine could not be introduced into the 4-position by a direct Mannich reaction. Alternatively, the corresponding dimethylamine derivatives **33a-c** were treated with 2-methylimidazole or guanidine in ethanol, and compounds **34a-c** were generated in good yields. These were reacted with sodium perborate tetrahydrate, and then compounds **34a-c** were oxidized into compounds **35a-c** as expected. This modified synthetic route resulted in a greater purity and yield of target compounds.

The synthetic route and structures of newly designed compounds ethyl 5-hydroxy-1*H*-indole-3-carboxylate derivatives were obtained as described in Scheme 1.

Chemistry

Melting points were measured with a Veego melting point apparatus and were uncorrected. Mass spectra (MS) were taken in ESI mode on Agilent 1100 LC-MS. ^{1}H NMR spectra were recorded using Brüker ARX-300, 300 MHz spectrometers with Me_4Si as an internal standard.

General procedure for the synthesis of compounds 34a-c Compounds **33a-c** (0.04 mol) were added to a solution of 2-methyl-1-imidazole or guanidine (0.2 mol) in anhydrous ethanol (100 ml) at 78°C with constant stirring. The solid dissolved about 1 hour later. The reaction mixture continued to stir with refluxing until a mass of solid appeared in the solution. The precipitate was filtered and dried to give the desired compounds **34a-c** (75-78%).

General procedure for the synthesis of compounds 35a-c Appropriate analogues of **34** (0.02 mol) were dissolved in galacial acetic acid (80 ml). Then, sodium perborate tetrahydrate (0.02 mol) was added into the solution. After stirring at 45~50 °C for 3-4 hours, most of the acetic acid was evaporated in vacuo. Finally, the solution was poured into water and the precipitate was filtered and washed by acetone to give compounds **35a-c** (83-88%).

Ethyl 6-bromo-1-methyl-4-((2-methyl-1 H-imidazol-1-yl) methyl)-2-((benzylsul- finyl)methyl)-5-hydroxy-1 H-indole-3-carboxylate (35a) Ethyl 6-bromo-1-methyl-4-((2-methyl-1 H-imidazol-1-yl)methyl)-2-((benzyl)thiomethyl)-5-hydroxy-1*H*-indole-3-carboxylate (0.02 mol) was first dissolved in galacial acetic acid (80 ml). Sodium perborate tetrahydrate (0.02 mol) was then added into the solution. After stirring at 45~50 °C for 3~4 hours, most of the acetic acid was evaporated in vacuo. Then the solution was poured into water and the precipitate was filtered and washed by acetone to give a white powder, compound **35a** (9.6 g, 88%). Mp:159-161°C; (DMSO-d_6): δ 0.95 (t, 3 H, J=7.2 Hz, -$OCH_2C\boldsymbol{H_3}$), 2.67 (s, 3 H, imidazolyl-C$\boldsymbol{H_3}$), 3.81 (t, 3 H, -N$C\boldsymbol{H_3}$), 3.95 (q, 2 H, J=7.2 Hz, -O$C\boldsymbol{H_2}CH_3$), 4.73-4.75 (m, 2 H, -C$\boldsymbol{H_2}$-phenyl), 5.16 (m, 2 H, -C$\boldsymbol{H_2}$-sulfinyl-benzyl), 5.68 (m, 2 H, -C$\boldsymbol{H_2}$N<), 6.88 (s, 1 H, -Φ***H***), 7.39~7.47 (m, 6 H, -Φ***H***, -Bz***H***), 8.07 (s, 1 H, -Φ***H***), 9.32 (br s, 1 H, active ***H***), 14.10 (br s, 1 H, active ***H***). MS: *m/z* 543.9, 545.8 [MH^+].

Ethyl 6-bromo-1-cyclopropyl-4-((2-methyl-1 H-imidazol-1-yl)methyl)-2-((2-fluo- robenzylsulfinyl)methyl)-5-hydroxy-1 H-indole-3-carboxylate (35b) White powder (9.5 g, 87%); Mp:166-168 °C; (DMSO-d_6): δ1.03 (m, 2 H, -N-CH($C\boldsymbol{H_2}$)$_2$), 1.11 (t, 3 H, -$OCH_2C\boldsymbol{H_3}$), 1.17 (m, 2 H, -N-CH($C\boldsymbol{H_2}$)$_2$), 2.70 (s, 3 H, imidazolyl-C$\boldsymbol{H_3}$), 3.19 (m, 1 H, -N-C***H***(CH_2)$_2$), 4.09 (q, 2 H, J=7.2 Hz, -O$C\boldsymbol{H_2}CH_3$), 4.11~4.26 (m,

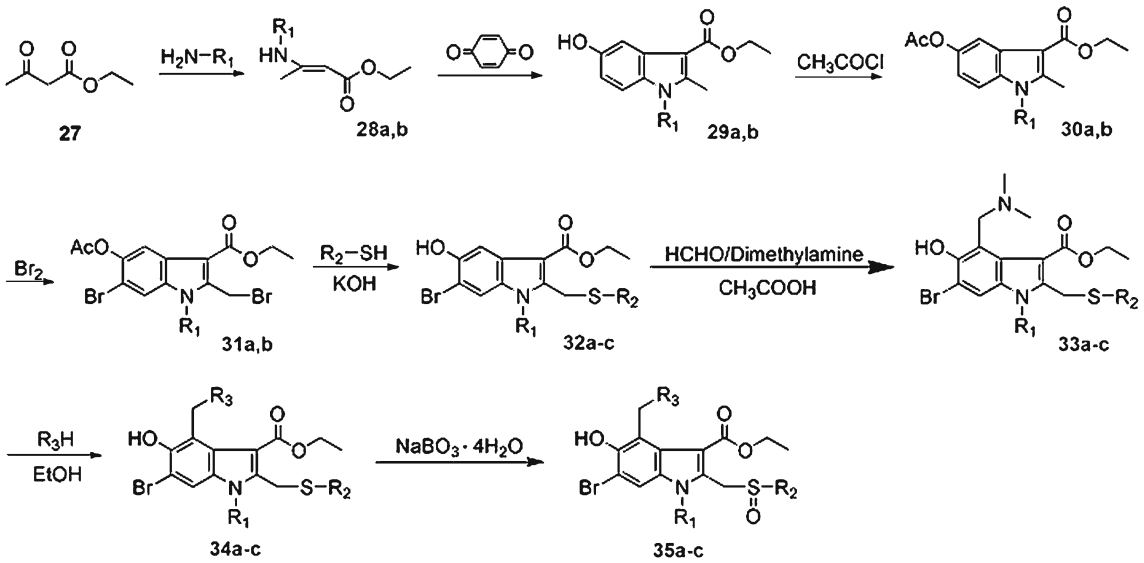

35a: R_1= Methyl, R_2= Benzyl, R_3= 2'-Methyl-1*H*-imidazol-1-yl;

35b: R_1= Cyclopropyl, R_2=2'-Fluorobenzyl, R_3= 2'-Methyl-1*H*-imidazol-1-yl;

35c: R_1= Methyl, R_2=2'-Methoxyphenyl, R_3= Guanidinyl.

Scheme 1 Synthetic route and structures of newly designed compounds

4 H, -C***H₂***-sulfinyl- C***H₂***-phenyl), 5.76 (m, 2 H, -C***H₂***N<), 6.73 (s, 1 H, -Φ***H***), 6.81 (s, 1 H, -Φ***H***), 7.30~7.38 (m, 3 H, -Bz***H***), 7.58~7.60 (m, 1 H, -Bz***H***), 7.89 (s, 1 H, -Φ***H***), 9.25 (br s, 1 H, active ***H***). MS: *m/z* 588.3, 590.2 [MH^+].

Ethyl 6-bromo-1-methyl-4-(guanidinylmethyl)-2-((2-methoxyphenyl)sulfinyl- methyl)-5-hydroxy-1 H-indole-3-carboxylate (35c) White powder (8.9 g, 83%); mp:174-176 °C; (DMSO-d_6): δ 1.29 (t, 3 H, J=7.2 Hz, -OCH$_2$C***H₃***), 3.61 (t, 3 H, -NC***H₃***), 3.73 (s, 3 H, 2'-OC***H₃*** of phenyl), 4.14 (q, 2 H, J=7.2 Hz, -OC***H₂***CH$_3$), 4.75~4.97 (m, 4 H, -C***H₂***N<, -sulfinyl-C***H₂***-), 6.75 (s, 2 H, -N***H₂***), 7.12~7.19 (m, 2 H, -CH$_2$N***H***, -Ph***H***), 7.25~7.55 (m, 3 H, -Ph***H***), 7.90 (s, 1 H, -Φ***H***), 9.18 (br s, 1 H, active ***H***). MS: *m/z* 536.9, 538.8 [MH^+].

Biological assay

Ex vivo anti-HBV assays

The antiviral activities of compounds **35a-c** against HBV in HepG2.2.15 cells were evaluated by methods reported elsewhere [13–18]. The ex vivo anti-HBV activities included the ability to inhibit the production of HBsAg and HBeAg and the replication of HBV DNA in HBV-infected 2.2.15 cells. For the antiviral analyses, confluent cultures of 2.2.15 cells (purchased from ATCC) were maintained in 96-well flat-bottomed tissue culture plates in RPMI 1640 medium with 2% fetal bovine serum [14, 15]. Cultures were treated with eight consecutive daily doses of the test compounds. Cells with media alone were used as the blank control, while lamivudine (purchased by Glaxo & Welcome Co.) was used as positive control. The media containing fresh test compounds and positive control was changed daily. HBV nucleic acid and protein levels were measured eight days after the first treatment. Extracellular HBV surface antigen (HBsAg) and HBV e antigen (HBeAg) levels produced from 2.2.15 cells were evaluated by semiquantitative enzyme immunoassay (EIA) methods using commercial kits (HBsAg, Abbott Laboratories; HBeAg, Diasorin, Inc.) as previously described [16]. Intracellular HBV DNA levels were measured by quantitative southern blot hybridization [15]. Based on the HBV DNA levels measured under eight doses, the IC_{50} and selected index of the evaluated compounds and lamivudine were calculated, respectively. Two independent experiments were established and the IC_{50} was the mean of two independent experiments.

Cytotoxicity assay

Cytotoxicity induced by the test compounds in cultured 2.2.15 cells was also determined. Briefly, 2.2.15 cells were grown to confluence in 96-well flat-bottomed tissue culture plates and treated with test compound (in 0.2 mL culture medium/well) as described above. Untreated control cultures were main-

tained on each 96-well plate. Toxicity was determined by measuring neutral red dye uptake, as determined from the absorbance at 510 nm relative to untreated cells. This was done 24 hours following day 9 of treatment.

Results and discussion

CoMFA

PLS analysis gave a correlation with a cross-validated r^2_{cv} of 0.689, with 3 optimum number of components. The non-cross-validated PLS analysis was repeated with the optimum number of components, as determined by the cross-validated analysis, to give r^2 of 0.965. These values indicate a good conventional statistical correlation and that the CoMFA model has a good predictive ability. The steric field descriptors (1170 variables) explain 57.1% of the variance, while the electrostatic descriptors explain 42.9%. The non-cross-validated calculations are shown in Fig. 2a.

CoMFA coefficient contour maps

The CoMFA steric contour map indicates areas in which steric bulk might have a favorable (green) or disfavorable (yellow) effect on the activity of an analogue. The analysis suggested that bulky groups are preferred at the R_2 position (Fig. 3). The yellow contour near the 4-position of the indole ring is observed indicating that small groups are favored in position R_3.

The CoMFA electrostatic map indicates red contours in regions where high electron density might play a favorable role in activity, and blue contours in areas in which the negative charged substituent is predicted to decrease activity. As shown in Fig. 3, the blue area surrounding the group of R_2 reflects the increase in activity found by introducing positive charged substituent in this region. In contrast, the red contour at the end of the group R_3 indicates that negative charged substituent is favored in this region.

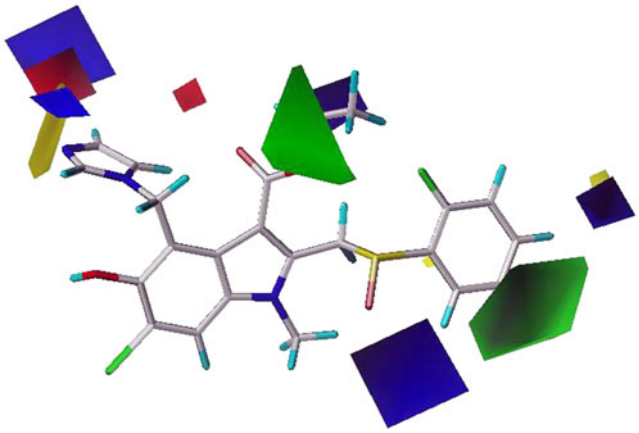

Fig. 3 Contour maps from the final CoMFA analysis in combination with all analogues of the training set. Green contours refer to sterically favored regions; yellow contours indicate disfavored areas. Blue contours refer to regions where negatively charged substituents are disfavored; red contours indicate regions where negatively charged substituents are favored. The molecule in center is compound **15**

CoMSIA

Using steric, electrostatic, hydrophobicity and H-bond acceptors as descriptors, a CoMSIA model with an r^2_{cv} value of 0.578 for five components, the optimum number of components, and a conventional r^2 of 0.973 was obtained.

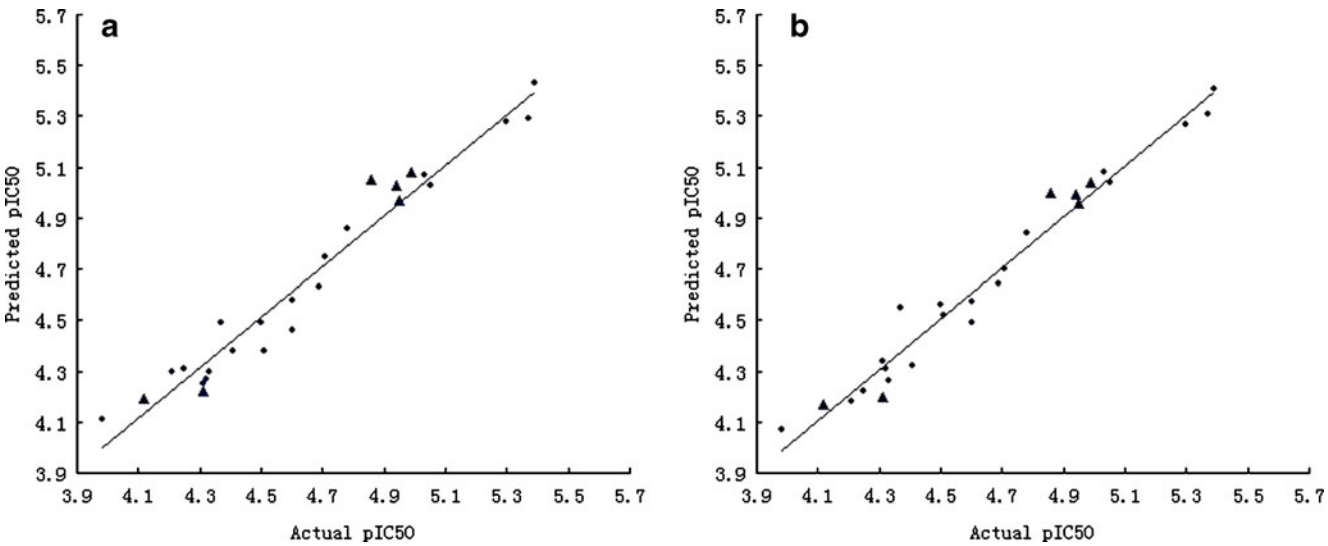

Fig. 2 Plot of observed pIC_{50} versus predicted activities (the data for the training set are marked as•, and testing set as▲). (**a**) Result from CoMFA. (**b**) Result from CoMSIA

Table 2 Experimental and calculated pIC_{50} of the studied and newly designed compounds

Compound.	pIC_{50}	*CoMFA*		*CoMSIA*	
		Predict	*Residual*	*Predict*	*Residual*
Training set					
1	4.21	4.30	−0.09	4.18	0.03
2	4.41	4.38	0.03	4.32	0.09
3	5.39	5.43	−0.04	5.41	−0.02
4	4.50	4.49	0.01	4.56	−0.06
5	4.51	4.38	0.13	4.52	−0.01
6	3.98	4.11	−0.13	4.07	−0.09
7	4.33	4.30	0.03	4.26	0.07
8	4.32	4.27	0.05	4.31	0.01
9	4.31	4.25	0.06	4.34	−0.03
10	5.05	5.03	0.02	5.04	0.01
11	4.71	4.75	−0.04	4.70	0.01
12	4.25	4.31	−0.06	4.22	0.03
13	5.03	5.07	−0.04	5.08	−0.05
14	5.30	5.28	−0.02	5.27	0.03
15	4.78	4.86	−0.08	4.84	−0.06
16	4.60	4.46	0.14	4.49	0.11
17	4.69	4.63	0.06	4.64	0.05
18	4.37	4.49	−0.12	4.55	−0.18
19	5.37	5.29	0.08	5.31	0.06
20	4.60	4.58	0.02	4.57	0.03
Test set					
21	4.94	5.03	−0.09	4.99	−0.05
22	4.99	5.08	−0.09	5.04	−0.05
23	4.86	5.05	−0.19	5.00	−0.14
24	4.95	4.97	−0.02	4.96	−0.01
25	4.12	4.19	−0.07	4.17	−0.05
26	4.31	4.22	0.09	4.20	0.11
Novel compounds					
35a	5.51	5.03	0.48	4.95	0.56
35b	5.29	5.11	0.18	5.13	0.16
35c	5.48	5.08	0.40	4.84	0.64

pIC_{50}: Lg $(1/IC_{50})$, IC_{50} is mol/l

The CoMSIA-predicted activities for these analogues are shown in Table 2. The CoMSIA model exhibited a good cross-validated correlation, indicating that it is also highly predictive. The steric field descriptors explain 15.8% of the variance, the electrostatic descriptor explain 33.1%, and the hydrophobic field explains 21.1% of variance. Here the additional H-bond acceptor explains the remaining 30.0% of variance, respectively. The statistical results of CoMFA and CoMSIA models were listed in Table 3.

CoMSIA coefficient contour maps

Figure 4a depicts steric contour maps of CoMSIA analysis in combination with all analogues of the training set. Sterically favored green regions were found on the phenyl ring of the arylsulfinyl group, whereas the sterically unfavored yellow region was found near the mannich base group in position 4 of the indole ring. This is consistent with the results from the CoMFA analysis, in which larger morpholino and 4-methylpiperazinyl groups would decrease the activity.

An inspection of the CoMSIA electrostatic coefficient contour map (Fig. 4b) shows correspondence to the CoMFA results (Fig. 3). The electrostatic field distribution is nearly the same as that of the CoMFA (Fig. 3). In the electrostatic contour map, negative charged substituent is favored in the red region, which was found far from the amino side chain nitrogen in position 4 of the indole ring. On the contrary, a favored positive charge or disfavored negative charge blue region was found near the same group. The result indicates negatively charged ring systems may decrease the activity, and increasing the positive charge in the mannich base group will benefit the anti-HBV activity. In addition, a blue contour polyhedral surrounding the atoms near the para-position of the arylsulfinyl group, whereas a red contour polyhedral surrounding the ortho-position of the same group appears in the CoMSIA map (Fig. 4b). This indicates that positive charges substituents in the para-position are favored in this region, and negative interactions in ortho-position. This is far from the sulfinyl group on the aryl ring where halide substitution was well tolerated.

Table 3 Statistical results of CoMFA and CoMSIA models

Model	q^2	SEE_{-cv}	r^2	***SEE***	***F***	*Field contribution*			
						steric	*electrostatic*	*hydrophobic*	*acceptor*
CoMFA	0.689	0.246	0.965	0.082	148.751	0.571	0.429		
CoMSIA	0.578	0.307	0.973	0.078	100.342	0.158	0.331	0.211	0.300

q^2 cross-validated correlation coefficient; SEE_{-cv}: the cross-validated standard errors; r^2 non-validated correlation coefficient; ***F***: the statistical square deviation ratio; ***SEE***: standard error of estimate

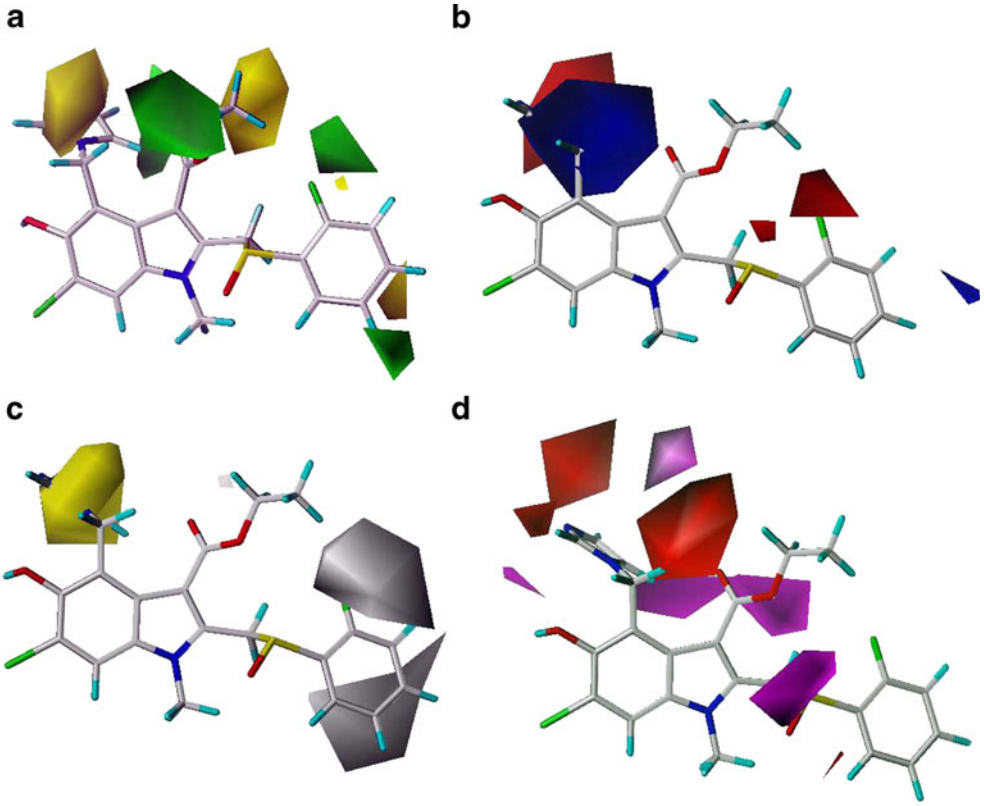

Fig. 4 Contour maps from the final CoMSIA analysis in combination with all analogues of the training set. (**a**) Steric coefficient contour map. Green contours refer to sterically favored regions; yellow contours indicate disfavored areas. (**b**) Electrostatic coefficient contour map. Blue contours refer to regions where negatively charged substituents are disfavored; red contours indicate regions where negatively charged substituents are favored. (**c**) Hydrophobic coefficient contour map. Yellow contours refer to regions where hydrophobic substituents are favored; white contours indicate regions where hydrophilic substituents are favored. (**d**) H-bond acceptor coefficient contour map. Magenta contours refer to regions where H-bond acceptor substituents are favored; red contours indicate regions where H-bond acceptor substituents are disfavored. The molecule in the center is compound **15**

One of the advantages of CoMSIA is that hydrophobic contributions, which can't be completely treated using Lennard-Jones and Coulombic fields, are evaluated using a hydrophobic similarity index field. In the hydrophobic coefficient contour map, regions in which enhanced hydrophilicity and hydrophobicity are favorable, are indicated by white and yellow, respectively. As shown in Fig. 4c, the end of substituent at 2-position is surrounded by a white polyhedral, which means that a more hydrophilic substituent in this region is beneficial to the activity. Yellow polyhedrals centralize on the atoms in position 4. Around these regions a hydrophobic substituent is favored.

The CoMSIA H-bond acceptor contour plot is presented in Fig. 4d. According to Fig. 4d, the magenta contour near the halogen on group substitution at 2-position indicates H-bond acceptor substituents are favored.

Validation of the strategy for 3D QSAR models

An important aspect of a QSAR model is the ability to quantitatively predict the relative activities of the other compounds not included in the training set. Compounds **21-26** (Table 1) were excluded from the training set to serve as test compounds to evaluate the predictive ability of the present CoMFA and CoMSIA models. The results for all compounds are summarized in Table 2, in which the observed anti-HBV activities predicted by our CoMFA and CoMSIA models are listed. The predicted values agreed remarkably well with the experimental results; the largest residual of both CoMFA and CoMSIA is -0.18, which shows that our model is able to accurately reproduce the results of the test compounds with the same experimental condition as training compounds. From the results, the CoMFA model seems to be more suitable to describe the analogues.

After the qualitative explanation on the experimental data, we designed three new analogues based on the information obtained from CoMFA and CoMSIA models,

Table 4 Anti-HBV activities of compounds $35_{a\text{-}c}$

Compd	$TC_{50}(\mu M)$ *	*HBV DNA replication*	
		$IC_{50}(\mu M)$ *	*SI*
35a	136.3	3.1	44.0
35b	257.0	5.1	50.4
35c	119.4	3.3	36.2
lamivudine	6976	994	7.0

*: all values are the mean of two independent experiments. TC_{50}: 50% cytotoxic concentration in HepG 2.2.15cells; IC_{50}: 50% inhibitory concentration; *SI*: selectivity index, TC_{50}/IC_{50};

and their anti-HBV activities were evaluated and listed in Table 4. The anti-HBV activity of compound **35a** (IC_{50}: 3.1 μM) is far greater than that of lamivudine, and even higher than the most potent reported compound **3** (IC_{50}: 4.1 μM). By employing a 2-methylimidazolyl group in position 4 of the indole ring, the electrostatic potential near that substituent is more positive in compound **35a** than in others. Moreover, sterically bulky groups like a benzyl ring in place of a phenyl ring group in position 2 (compound **18**, IC_{50}: 42.5 μM), showed a favorable effect. Compound **35c** displayed anti-HBV activity (IC_{50}: 3.3 μM) quite similar to compound **35a**. Compared with compound **12** (IC_{50}: 56.0 μM), the methoxy group of **35c** increased the positive charges on the aryl ring of the 2-position. Small groups with positive charge such as guanidinyl group in position 4 also enhanced its anti-HBV activity (compound **19**, IC_{50}: 4.3 μM). As shown in Table 1, a cyclopropyl group instead of a methyl group in position 1 would benefit anti-HBV activities (compound **12** vs **13** (IC_{50}: 56.0 vs 9.4 μM), compound **16** vs **17** (IC_{50}: 25.4 vs 20.3 μM)). More negative charged substituent in the ortho-position of the sulfonyl aryl ring may increase the activity. Halide substitution with a fluorine atom was done based on the above information. The newly designed compound **35b**, with IC_{50} 5.1 μM, also exhibited excellent anti-HBV activity. Although the sulfonyl group in place of sulfinyl group in position 2 increased anti-HBV activity (compound **2** vs **3**, IC_{50}: 39.3 vs 4.1 μM), the toxicity of compound increased simultaneously (compound **2** vs **3**, TC_{50}: 494.1 vs 40.0 μM). Therefore the sulfinyl group was introduced into position 2 of the newly designed compounds.

Pharmacological activities of newly synthesized compounds

Based on the information derived from 3D QSAR models, target compounds **35a-c** were synthesized and evaluated for their anti-HBV activities, namely the ability to inhibit the replication of HBV DNA and the production of HBsAg and HBeAg in HBV-infected 2.2.15 cells. The antiviral activities of compounds **35a-c** against HBV in 2.2.15 cells were evaluated by methods reported by Sells and Korba [14–16]. The IC_{50} and selected index of the evaluated compounds and lamivudine were calculated respectively. Cytotoxities induced by the test compounds and positive control in cultures of 2.2.15 cells were also determined and were presented with TC_{50}. The results were summarized in Table 4.

From the pharmacological results, it was found that compound **35a** showed the most potent ex vivo anti-HBV activity (IC_{50}: 3.1 μM, SI: 44.0). With IC_{50} values of 5.1 μM and 3.3 μM respectively, compound **35b** and **35c** are far more potent than the control lamivudine (IC_{50}: 994 μM).

Conclusions

CoMFA and CoMSIA methods were successfully used in our study to build 3D QSAR models based on 5-hydroxy-1*H*-indole-3-carboxylates possessing anti-HBV activities. The CoMFA and CoMSIA models proved to have good predictive ability. In addition, the information obtained from CoMFA and CoMSIA maps were used for further design and insight into 5-hydroxy-1*H*-indole-3-carboxylates. Combining the clues derived from the 3D QSAR and further validation of the 3D QSAR models, the anti-HBV activities of the newly synthesized indole derivatives were well accounted for. It can also be used for our future studies on the 5-hydroxy-1*H*-indole-3-carboxylates derivatives.

Acknowledgments We greatly thank the helpful comments on this manuscript from Dr. Daniela Fera from the University of Pennsylvania. We gratefully acknowledge financial support from the National Natural Science Foundation of China (Grant 30901844 and 20972174), the Science and Technology Foundation of Guizhou Province (Grant [2008] 2142 and [2008]2253), the State Key Program of Basic Research of China grant (2009CB918502), Shanghai Committee of Science and Technology grant (10410703900 and 0843190800), National S&T Major Project (2009ZX09501-001), State Key Laboratory Grant (SIMM1004KF-15) and Guangdong Science and Technology Department (2010A030100006).

References

1. Ganem D (2004) Hepatitis B virus infection–natural history and clinical consequences. New Engl J Med 350:1118–1129
2. Rerknimitr RMK, Nusont MB, Mahachai V, Kullavanijaya P (2004) Result of endoscopic biliary drainage in hilar cholangiocarcinoma. J Clin Gastroenterol 38:518–523
3. Humphries JSD (2003) Antivirals for the treatment of chronic hepatitis B:current and future options. Intervirology 46:413–420
4. Woodland AM (2006) Entecavir:a new nucleoside analog for the treatment of chronic hepatitis B Infection. Pharmacotherapy 26:1745–1757
5. Colonno RJR, Baldick CJ, Levine S, Podornowski K, Yu CF, Walsh A, Fang J, Hsu M, Mazzucco C, Eggers B, Zhang S, Plym M, Klesczewski K, Tenney DJ (2006) Entecavir resistance is rare in nucleoside naïve patients with hepatitis B. Hepatology 44:1656–1665
6. Chai HF, Zhao YF, Zhao CS, Gong P (2006) Synthesis and in vitro anti-hepatitis B virus activities of some ethyl 6-bromo-5-hydroxy-1*H*-indole-3-carboxylates. Bioorg Med Chem 14:911–917
7. Zhao CS, Zhao YF, Chai HF, Gong P (2006) Synthesis and in vitro anti-hepatitis B virus activities of some ethyl 5-hydroxy-1*H*-indole-3-carboxylates. Bioorg Med Chem 14:2552–2558
8. Zhao CS, Zhao YF, Chai HF, Gong P (2006) Synthesis and in vitro anti-hepatitis B virus activities of several ethyl 5-hydroxy-1*H*-indole-3-carboxylates. Chem Res Chin Univ 22:577–583
9. aSYBYL [computer program]. Version 6.8. St Louis (MO):Tripos Associates
10. Ghose A, Crippen G (1986) Atomic Physicochemical parameters for three-dimensional structure-directed quantitative structure-activity relationships I. Partition coefficients as a measure of hydrophobicity. J Comput Chem 7:565–577
11. Monti SA (1966) The Nentizescu condensation of ethyl 3-aminocrotonate and 1, 4-benzoquinone. J Org Chem 31:2669–2672

12. Grinev AN, Pershin GN (1990) 5-hydroxyindole-3-carboxylates derivatives and their use. WO 9008135
13. Sells MA, Chen ML, Acs G (1987) Production of hepatitis B virus particles in Hep G2 cells transfectd with cloned hepatitis B virus DNA. Proc Natl Acad Sci USA 84:1005–1009
14. Sells MA, Zelent AZ, MGAcs S (1988) Replicative intermediates of hepatitis B virus in HepG2 cells that produce infectious virions. J Virol 62:2836–2844
15. Korba BE, Gerin JL (1992) Use of a standardized cell culture assay to assess activities of nucleoside analogs against hepatitis B virus replication. Antivir Res 19:55–70
16. Korba BE, Gerin JL (1995) Antisense oligonucleotides are effective inhibitors of hepatitis B virus replication in vitro. Antivir Res 28:225–242
17. Lv ZL, Sheng CQ, Wang TT, Zhang YK, Liu J, Feng JL, Sun HL, Zhong HY, Niu CJ, Li K (2010) Design, synthesis, and antihepatitis B virus activities of novel 2-pyridone derivatives. J Med Chem 53:660–668
18. Zhang Q, Jiang ZY, Luo J, Liu JF, Ma YB, Guo RH, Zhang XM, Zhou J, Chen JJ (2009) Anti-HBV agents. Part 2:synthesis and in vitro anti-hepatitis B virus activities of alisol A derivatives. Bioorg Med Chem Lett 19:2148–2153